AGU PUBLICATIONS

JGR

Journal of Geophysical Research: Space Physics

RESEARCH ARTICLE

10.1002/2015JA021960

Edge of polar cap patches

K. Hosokawa[1,2], S. Taguchi[3], and Y. Ogawa[4,5]

[1]Department of Communication Engineering and Informatics, University of Electro-Communications, Tokyo, Japan, [2]Center for Space Science and Radio Engineering, University of Electro-Communications, Tokyo, Japan, [3]Department of Geophysics, Graduate School of Science, Kyoto University, Kyoto, Japan, [4]National Institute of Polar Research, Tokyo, Japan, [5]Department of Polar Science, SOKENDAI (Graduate University for Advanced Studies), Kanagawa, Japan

Key Points:
- Fingerlike signatures of plasma instability are identified within polar cap patches
- Gradient in the leading edge of patches is sharper than that in the trailing edge
- Plasma mixing through the plasma instability determines the shape of patches

Supporting Information:
- Supporting Information S1
- Animation S1

Correspondence to:
K. Hosokawa,
keisuke.hosokawa@uec.ac.jp

Citation:
Hosokawa, K., S. Taguchi, and Y. Ogawa (2016), Edge of polar cap patches, *J. Geophys. Res. Space Physics*, *121*, 3410–3420, doi:10.1002/2015JA021960.

Received 28 SEP 2015
Accepted 10 MAR 2016
Accepted article online 14 MAR 2016
Published online 6 APR 2016

Abstract On the night of 4 December 2013, a sequence of polar cap patches was captured by an all-sky airglow imager (ASI) in Longyearbyen, Norway (78.1°N, 15.5°E). The 630.0 nm airglow images from the ASI of 4 second exposure time, oversampled the emission of natural lifetime (with quenching) of at least ~30 sec, introduce no observational blurring effects. By using such high-quality ASI images, we succeeded in visualizing an asymmetry in the gradients between the leading/trailing edges of the patches in a 2-D fashion. The gradient in the leading edge was found to be 2–3 times steeper than that in the trailing edge. We also identified fingerlike structures, appearing only along the trailing edge of the patches, whose horizontal scale size ranged from 55 to 210 km. These fingers are considered to be manifestations of plasma structuring through the gradient-drift instability (GDI), which is known to occur only along the trailing edge of patches. That is, the current 2-D observations visualized, for the first time, how GDI stirs the patch plasma and such a mixing process makes the trailing edge more gradual. This result strongly implies a close connection between the GDI-driven plasma stirring and the asymmetry in the large-scale shape of patches and then suggests that the fingerlike structures can be used as markers to estimate the fine-scale structure in the plasma flow within patches.

1. Introduction

During prolonged intervals of southward interplanetary magnetic field (IMF), large-scale blobs (~1000 km horizontal extent) of enhanced electron density are often observed at the *F* region altitude in the polar cap ionosphere [*Weber et al.*, 1984]. Such regions of elevated electron density are called polar cap patches [*Carlson*, 2012, and references therein]. The dynamical features of patches have been investigated extensively by using various observations such as ionosondes, coherent HF radars, incoherent scatter radars, and GPS-total electron content [*Crowley*, 1996]. Patches are considered to be initiated on the dayside, probably near the dayside cusp region, and after the generation, they propagate toward the nightside all the way across the central polar cap region [e.g., *Oksavik et al.*, 2010]. In the past, it was demonstrated that patches can survive in the dark hemisphere for at least several hours due to slow recombination in the *F* region [*Hosokawa et al.*, 2011], which makes patches visible even in the nightside polar cap region [*Hosokawa et al.*, 2006]. Such a long lifetime and resulting long-distance travel of patches can introduce several space weather impacts on the satellite communication links (e.g., GPS) through the polar cap ionosphere [*Moen et al.*, 2013]. In particular, patches are considered to be primary sources of ionospheric scintillation at high latitudes [*Prikryl et al.*, 2013] because they are almost always accompanied by small-scale plasma density irregularities [*Hosokawa et al.*, 2009]. To better understand the characteristics of patch-associated irregularities and scintillation, it is highly desirable to observe the structure of patches in a two-dimensional (2-D) fashion and then to reveal what processes determine their characteristic shape.

In recent years, high-resolution 2-D 630.0 nm airglow measurements with all-sky imagers (ASIs) have been in use for visualizing the structuring process of polar cap patches [*Hosokawa et al.*, 2013, 2014]. A 630.0 nm airglow has a natural emission lifetime of ~2 min. Considering the quenching effect by nitrogen molecules, an actual emission lifetime would be 30–90 s at the typical altitudes of patches. This means that longer exposure time (e.g., 60 s) 630.0 nm airglow measurements suffer from smearing effect and cannot be used for imaging fine-scale structure of patches. In addition, patches tend to move rapidly with the background convection velocity (typically ~500 m s^{-1}) which would also introduce blurring of airglow images. For these reasons, short exposure time optical measurements are highly desired to visualize detailed structuring processes of polar

cap patches. By using 4 s exposure time 630.0 nm airglow measurements in Longyearbyen, Norway, *Hosokawa et al.* [2013] identified characteristic undulating structure in the trailing edge of patches, whose scale size was as small as 50 km. They claimed that the appearance of such features along the trailing edge is an indication of ongoing plasma structuring through the gradient-drift instability (GDI) [*Keskinen and Ossakow*, 1983]. This observation is in good agreement with an earlier work by *Kivanc and Heelis* [1997] who showed, by using DE-2 satellite ion density measurements, that the power of small-scale density structures is slightly higher on the trailing edge of patches. As predicted in computer simulations by *Gondarenko et al.* [2003], if such a structuring process is actually operative in the trailing edge, the shape of patches should be asymmetric between the leading and trailing edges. In the previous literature, actually, several low-altitude satellite observations have revealed that the gradient in the trailing edge of patches is more gradual than that in the leading edge [e.g., *Coley and Heelis*, 1998]. However, such in situ density measurements by satellites are basically 1-D slices of patches; thus, the link between the occurrence of GDI and resulting asymmetric shape of patches has not been clarified in detail.

During the interval studied by *Hosokawa et al.* [2013], there were slight indications that the gradient in the leading edge was slightly steeper than that in the trailing edge. However, since the horizontal separation between the patches was very small (a few tens of kilometers), it was difficult to confirm the possible connection between the plasma structuring along the trailing edge and the asymmetry in the gradient between the edges. To clarify this point, it is highly demanded to investigate the edges of well-separated patches identified during an extended interval of southward IMF. For this purpose, we have surveyed four seasons of ASI data from Longyearbyen, Norway, and found a 4 h period containing 10 individual patches (temporal separation between the patches was ~20 min), which is ideal for estimating the edge gradients without contaminations from adjacent patches. In addition, characteristic undulating structures were again observed along the trailing edge of the patches. In this paper, by showing the ASI images from the above mentioned interval, we discuss the possible connection between the asymmetric shape of patches and ongoing plasma structuring through GDI.

2. Experimental Setup

We employed data from an all-sky airglow imager (ASI) in Longyearbyen, Norway (78.2°N, 15.6°E; AACGM latitude 75.3°), which has been operational since October 2011 [*Taguchi et al.*, 2012]. An EMCCD camera of Hamamatsu Photonics (C9100-13) is used as an imaging part of the ASI which has 512×512 spatial resolution. The ASI mainly takes all-sky images of the oxygen red-line emission at a wavelength of 630.0 nm, which allows us to visualize the electron density in the *F* region ionosphere in a two-dimensional fashion. The 630.0 nm images are taken with an exposure time of 4.0 s; thus, ~14 images are obtained every minute. We also observe the oxygen green-line emission at a wavelength of 557.7 nm once every minute with an exposure time of 1.0 s by rotating the filter turret. In the present study, we only use the 630.0 nm emission (OI, emission height of 200–300 km) as a proxy for the electron density at the *F* region altitude and visualize the two-dimensional structure of polar cap patches. In order to minimize the contribution of the background continuum emission from the sky, images at a wavelength of 572.5 nm are sampled every 10 min and used to derive the absolute emission intensity in Rayleigh following a method introduced in *Shiokawa et al.* [2009].

3. Observations

During a 4 h interval from 1900 to 2300 UT on 4 December 2013, a sequence of polar cap patches was observed to propagate across the field of view (FOV) of the ASI in Longyearbyen. Figure 1d demonstrates the temporal variation of the 630.0 nm airglow intensity in a format of keogram, which is a time series of the optical data extracted along the south to north cross section. The bright optical feature distributed in the equatorward half of the FOV is a manifestation of the main auroral oval on the nightside. The poleward edge of the auroral oval sometimes reached the zenith of Longyearbyen for example at around 1950 UT. During most of the interval, however, the bright auroral emission was located well equatorward of Longyearbyen, which allowed the ASI to detect weak airglow enhancements due to passages of patches. During a 3 h interval from 2000 to 2300 UT, 10 signatures of patches, which are denoted as A to J, were observed as traces of weak 630.0 nm airglow emission in the keogram. These traces first emerged from the northern edge of the FOV, subsequently propagated southward, and eventually dived into the poleward boundary of the auroral oval. This equatorward motion of the airglow features is a manifestation of the well-known antisunward transportation of patches in the polar

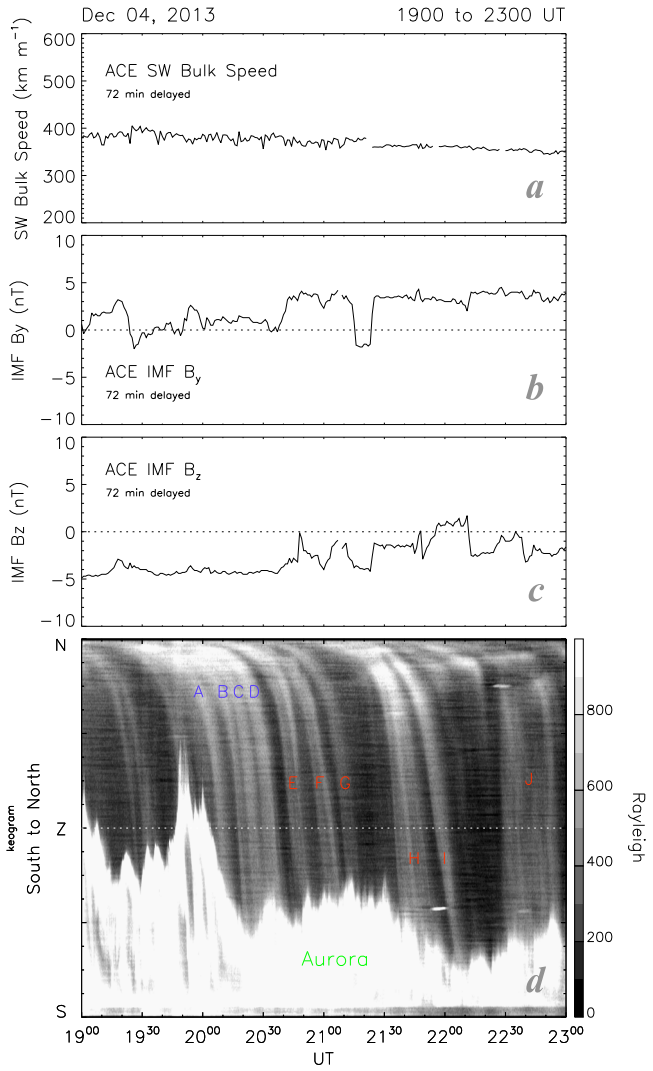

Figure 1. (a) Solar wind speed, (b) IMF B_y, and (c) B_z obtained from the ACE spacecraft during a 4 h interval from 1900 to 2300 UT on 4 December 2013. The time series is shifted by 72 min to account for the solar wind propagation delay from the spacecraft to the dayside polar cap, (d) Keogram reproduced from 630.0 nm all-sky images along the S–N cross section.

cap on the nightside. At the time of the passages of patches, the 630.0 nm airglow intensity increased to 300–450 R, which was approximately 2–3 times brighter than that in the surrounding dark area between the patch traces. The separation between the traces of patches was 20 min on average because 10 enhancements of airglow intensity were seen near the zenith during the 3 h interval from 2000 to 2300 UT.

Figure 1a gives the solar wind speed obtained from the ACE satellite situated ~220 R_E upstream of the Earth's magnetosphere. The solar wind speed was almost stable between 350 and 400 km s^{-1}. Figures 1b and 1c, respectively, show the IMF B_y and B_z components also obtained by the ACE satellite. Following a method documented in *Khan and Cowley* [1999], we estimated the solar wind time delay from the satellite to the dayside ionosphere to be 72 min. In this calculation, we used an average solar wind speed of ~370 km s^{-1} and a proton density of ~3 cm^{-3} (now shown). In Figures 1a–1c, the time series of the solar wind parameters have been shifted with this propagation time. The IMF B_y was mostly positive during the interval of interest. The IMF B_z was predominantly negative especially during the first 2 h of the interval, which is a suitable condition for the production of patches on the dayside and subsequent antisunward propagation. In general, the convective advection of patches from the cusp toward the central polar cap on the nightside takes 1–2 h; thus, the patches observed in Longyearbyen during the 3 h interval from 2000 to 2300 UT had been produced during the period of relatively strong southward IMF in the first half of the interval (1900–2100 UT).

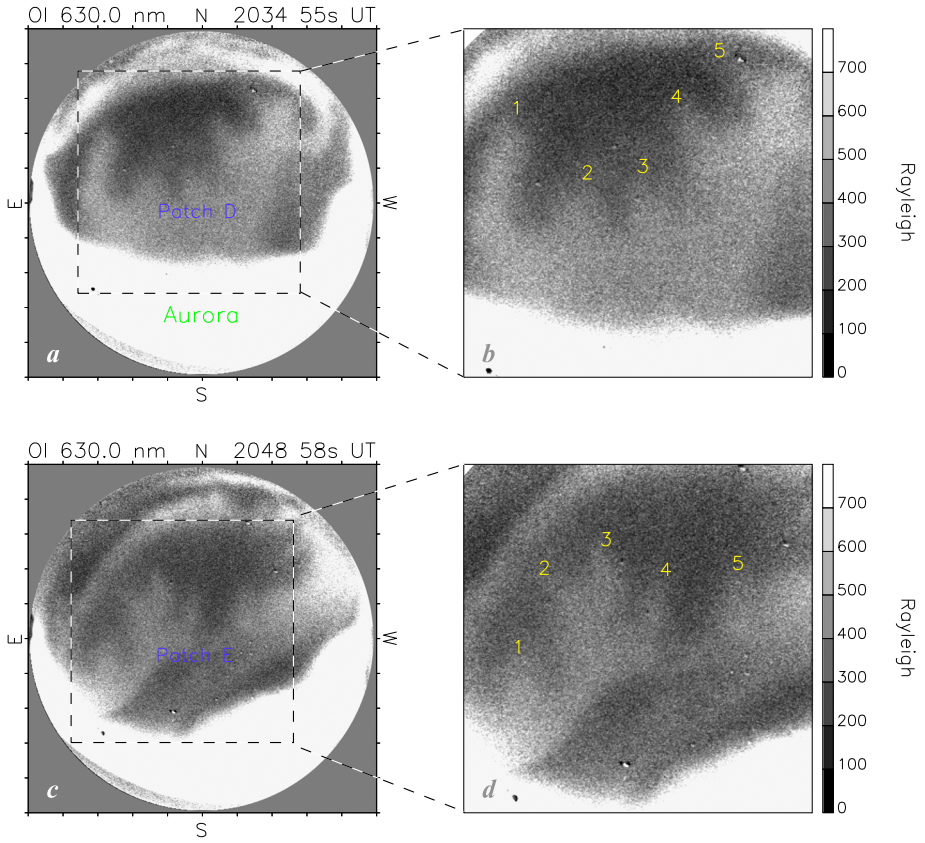

Figure 2. (a) The 630.0 nm all-sky airglow image recorded at ~2035 UT, (b) Zoom-up image of Figure 2a, (c) 630.0 nm all-sky airglow image recorded at ~2049 UT, (d) Zoom in image of Figure 2c.

During the interval shown in Figure 1, several interesting characteristics of patches were identified, which are introduced in Figures 2 and 3 by showing representative two-dimensional ASI images. Figure 2a gives an all-sky image at ~2035 UT, at which patch D was located near the zenith and drifting southwestward. The horizontal structure of the patch was more elongated in the direction perpendicular to its southwestward motion, that is one of the common characteristics of patches [*Hosokawa et al.*, 2014]. Although the airglow measurement in the equatorward portion of the FOV was significantly contaminated by an active aurora developing poleward, the trailing edge of patch D was nicely captured in the middle of the ASI image. Interesting to note is that patch D shows fingerlike structures along its trailing edge, which are more clearly seen in a zoom-in image in Figure 2b. At least five outstanding fingers are seen to originate from the trailing edge, as marked by the yellow numbers. The separation between the fingers ranges from 50 to 100 km. *Hosokawa et al.* [2013] have already reported an existence of undulating airglow structures having similar scale size along the trailing edge of patches, which were interpreted as manifestations of GDI. Although the fingerlike features seen during the current interval are very similar to the ones reported by *Hosokawa et al.* [2013], their spatial structures are more clearly identified in two-dimensional fashion. Figures 2c and 2d present the 2-D structure of patch E in an image taken at ~2049 UT. Similar fingerlike undulations are seen along the trailing edge of the patch as marked by the yellow numbers. A movie showing the successive passages of the patches between 1900 UT and 2300 UT is provided in the supporting information of this article (Animation S1). The animation demonstrates several indications of the fingerlike structure along the trailing edges for many of the patches during the interval of interest.

Another interesting feature of the patches is that the horizontal gradient in the optical intensity was clearly asymmetric between their leading and trailing edges. Figures 3a and 3b, respectively, show ASI images at ~2135 UT and 2158 UT. At ~2135 UT (Figure 3a), patch H was approaching the zenith and its leading edge was captured in the middle of the FOV. The boundary of the leading edge looks very sharp, while the trailing edge near the horizon seems somewhat diffuse. This tendency is more clearly seen in the image at ~2158 UT (Figure 3b). At this time, both the leading and trailing edges of patch I were captured near the zenith in a

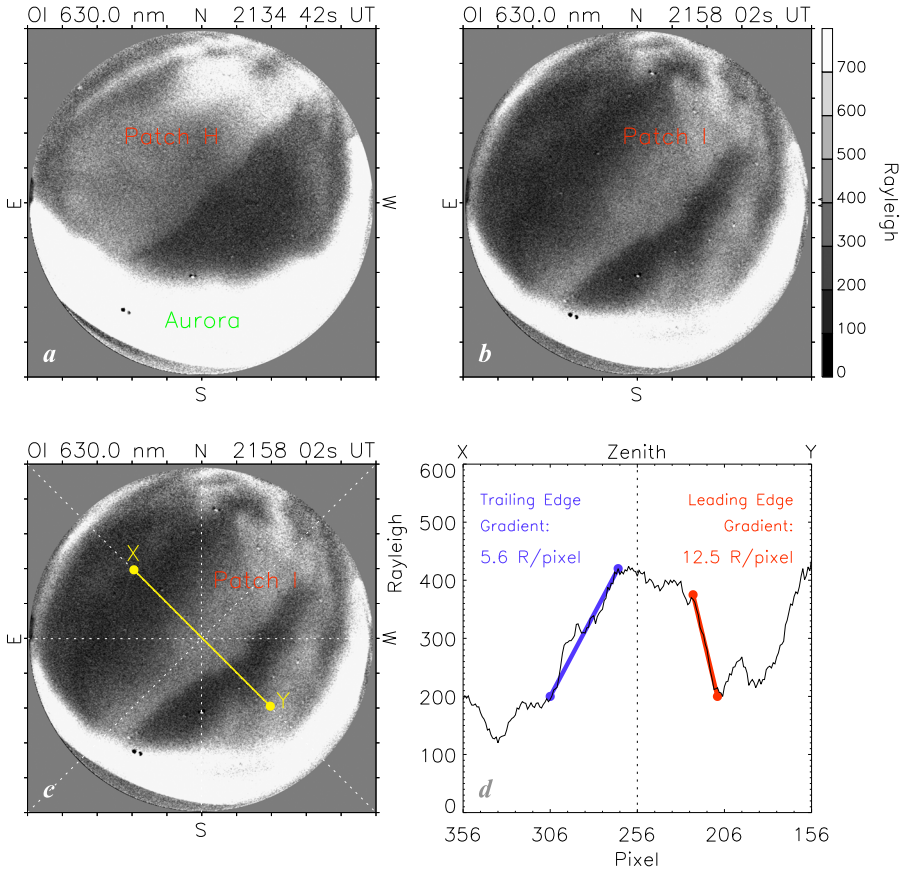

Figure 3. (a) The 630.0 nm all-sky airglow image recorded at 2135 UT, (b) 630.0 nm all-sky airglow image recorded at 2158 UT, (c) 630.0 nm all-sky airglow image recorded at 2158 UT, (d) Profile of the optical intensity along the yellow line in Figure 3c.

single all-sky image. There is an indication of asymmetry in the sharpness of the leading and trailing edges. In order to further confirm this characteristics, we plot a slice of the ASI image along a line roughly parallel to the moving direction of the patch. Figure 3d shows the optical intensity profile along the yellow line indicated in Figure 3c. In this panel, the horizontal axis is the pixel number and the pixel number 256 corresponds to zenith. As traced by the red and blue lines, the leading edge is clearly steeper than the trailing edge. The density gradient in the leading (trailing) edge of the patch is ~12.5 R pixel^{-1} (~5.6 R pixel^{-1}), which means that the gradient in the leading edge is ~2.2 times steeper than that in the trailing edge. Thus, there existed a certain level of asymmetry in the gradient between the leading and trailing edges.

In order to confirm the asymmetry in the gradient between the edges shown in Figure 3, we have estimated the gradient in the edges for all the 10 patches during the present interval. Figure 4a gives a time series of the 630.0 nm airglow intensity at zenith. In this interval, 10 outstanding peaks are identified in the optical intensity, which are manifestations of the passages of patches A to J. For some of the patches, for example, patches F, H, and J, the enhancement is composed of multiple peaks, which may be a signature of superposition of individual patches. In this analysis, however, we have treated such patches having multiple peaks as a single structure. For all the patches, we have traced the gradients in the leading and trailing edges, which are marked by the red (leading) and blue (trailing) lines in Figure 4b. Figure 4c shows the same time series during a 1 h interval from 2120 to 2220 UT, during which patches H and I passed the zenith of Longyearbyen. It is clearly seen that the gradients in the leading edges are steeper than those in the trailing edges. As shown in the keogram in Figure 1d, the traces of patches are straight near the zenith. This means that the patches did not change their moving speed drastically when they passed through the zenith. Hence, the gradients estimated from the temporal variation in the 630.0 nm emission intensity at zenith are reasonable proxies for the spatial gradient at the leading/trailing edges.

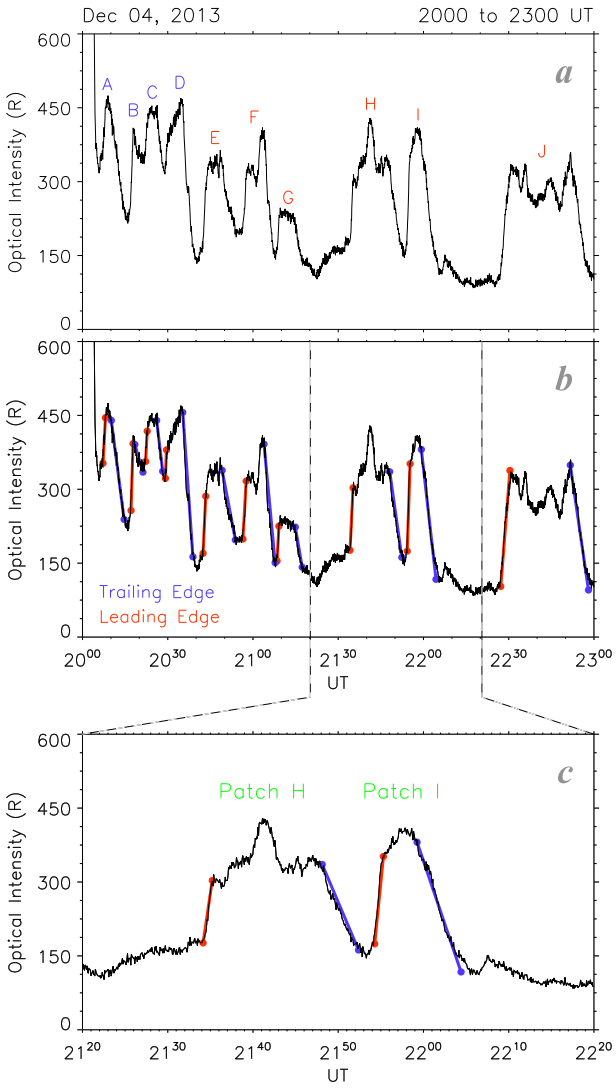

Figure 4. (a) Time series of the 630.0 nm airglow intensity at zenith. (b) Same data as those shown in Figure 4a, but gradients are traced for the leading (red) and trailing (blue) edges of the patches. (c) Zoom in of the time series for an interval from 2120 to 2220 UT. Again, the leading and trailing edges are traced by the red and blue lines, respectively.

4. Discussion

As shown in Figure 2, characteristic fingerlike structures were observed along the trailing edge of patches. Past computer simulations have already demonstrated that fingerlike structuring should occur in the trailing edge of patches [e.g., *Gondarenko et al.*, 2003]. However, the existence of such fingerlike features along the trailing edge has never been visualized in 2-D by using any observational techniques. Thus, we challenged it by improving the temporal resolution of airglow measurements with a high sensitive EMCCD camera, and then we succeeded in capturing clear 2-D images of the fingerlike structure. In addition, we showed that such a structuring process occurred only along the trailing edge. That is, the current observation gave a direct evidence for the structuring of patch shape through plasma instability and showed that such a process actually takes place only along the trailing edge of patches.

In the previous section, it was demonstrated that the gradient in the leading edge of the patches is clearly steeper than that in the trailing edge, at least for patches H and I (Figure 4c). To investigate the asymmetry in a more quantitative way, in Figure 5, we show the relationship between the gradient in the leading edge ($grad_L$) and that in the trailing edge ($grad_T$) estimated for all the 10 patches (patches A to J). In this analysis, we assumed that the horizontal propagation speed of the patches was stable at ~500 m s^{-1} and have

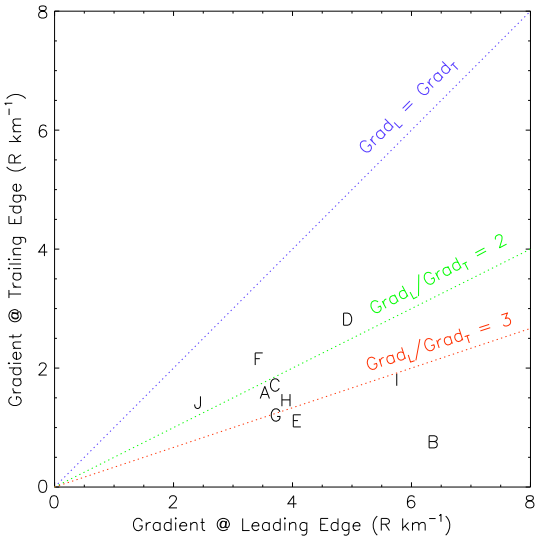

Figure 5. Relationship between the gradient in the leading (grad$_L$) and trailing (grad$_T$) edges.

converted the temporal variation of the airglow intensity in Figure 4 to the spatial gradient across the edges of the patches. The employed speed of the patches was directly derived from the orientation of the patch traces in the SW–NE aligned keogram assuming the 630.0 nm emission height of 250 km. Figure 5 shows that the ratio of grad$_L$ to grad$_T$ is around 2–3 for all the patches; thus, the gradient in the leading edge is systematically steeper than that in the trailing edge. In the past literature, *Coley and Heelis* [1998] investigated the edges of 72 polar cap patches detected by the DE-2 satellite and demonstrated that the gradient in the leading edge was, in average, 67% larger than the trailing edge. Later, *Gondarenko et al.* [2003] tried to reproduce this asymmetric characteristics by using three-dimensional nonlinear simulations of patch plasma. In their simulation, the trailing edge of patches is longer by a factor of 2 due to the turbulence-driven transport through plasma instabilities. Our observation of the gradient is generally consistent with these previous measurements and simulations, although the obtained ratio of grad$_L$ to grad$_T$ is slightly larger than the values in the past studies. In the analysis of *Coley and Heelis* [1998], gradients are estimated without knowing the spatial structure of patches; thus, it was not always guaranteed that the satellites sampled the slices of patches in the direction of patch motion. In contrast to this, in our analysis, we captured the asymmetric gradients from 2-D image in a direct manner (Figures 3c and 3d). In this sense, the current observation proved the asymmetric nature of patch edges without any assumptions.

In the following, we discuss the mechanism responsible for the observed asymmetry in the gradient between the leading and trailing edges of the patches. As shown in Figures 2, the shorter exposure time ASI measurement was succeeded in capturing fingerlike structures in the trailing edge of patches. *Hosokawa et al.* [2013] implied that generation of such fingers can be explained by plasma structuring through GDI. One of the primary reasons for this interpretation is that the appearance of fingers only in the trailing edge is in good agreement with the GDI mechanism because GDI is unstable only along the trailing edge of patches [e.g., *Milan et al.*, 2002]. *Hosokawa et al.* [2013] also demonstrated that the linear growth rate of GDI estimated from the simultaneous electron density measurement by the EISCAT Svalbard radar was consistent with the measured growth time of the structures. If the above mentioned structuring mechanism is operative, stirring of patch plasma should be much more effective across the GDI-unstable trailing edge of patches. Such a plasma mixing process could make the trailing edge more diffuse as patches propagate further toward the nightside. In contrast, the leading edge of patches is GDI stable because the electron density gradient is antiparallel to the background plasma drift which is not a favorable condition for the GDI waves to grow; thus, the leading edge should remain sharp for a long time. The current 2-D measurement of patches well visualizes how this scenario works, i.e., how the asymmetric occurrence of GDI produces the difference in the gradient between the leading and trailing edges of patches.

Generation mechanism of patch-associated plasma irregularities has been a central issue in the ionospheric research in the polar cap region, because such small-scale density structures are known to be one of the major

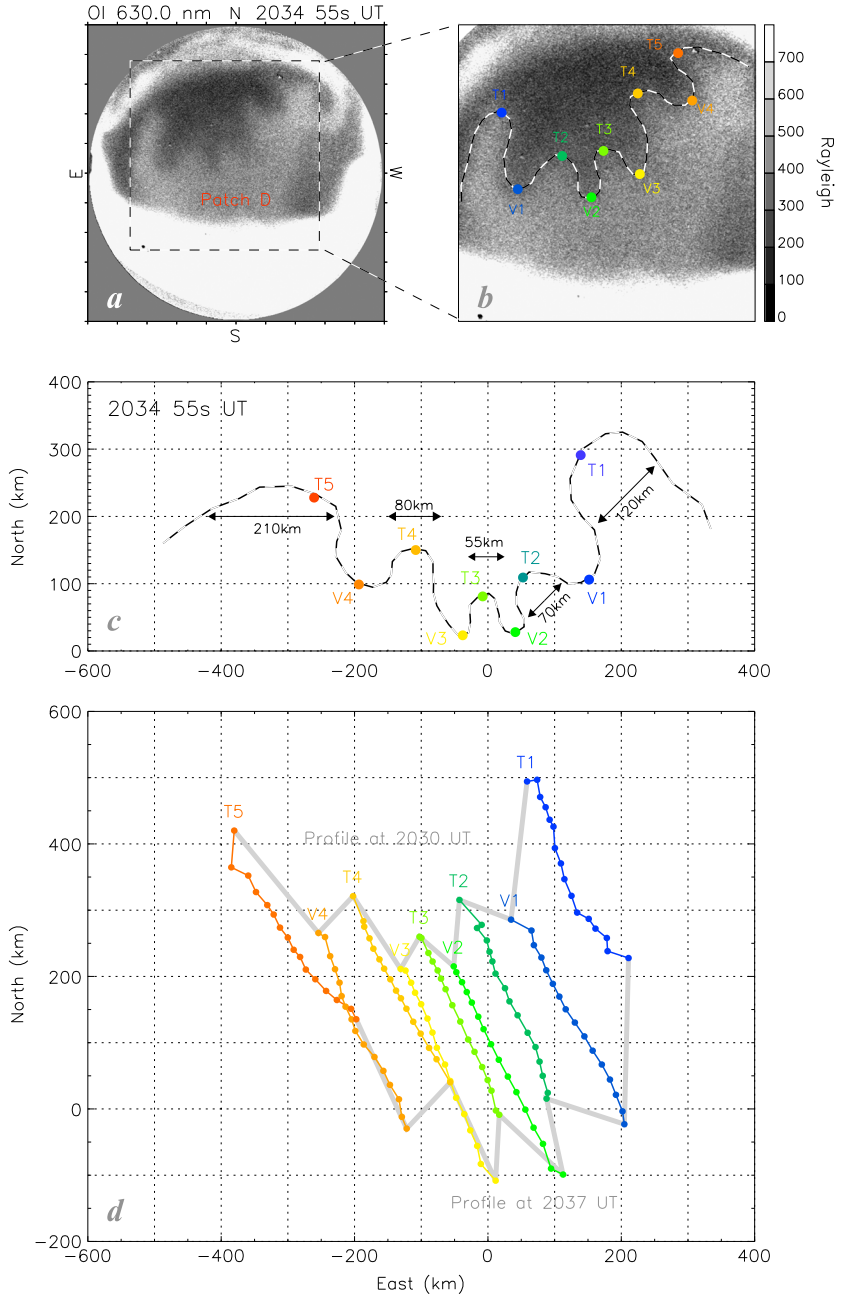

Figure 6. (a) The 630.0 nm all-sky airglow image recorded at 2135 UT, (b) zoom in image of Figure 6a where the traced outline of the trailing edge, tips (T1 to T5) and valleys (V1 to V4) of the fingers are indicated. (c) Outline of the trailing edge at 2035 UT mapped onto the horizontal plane assuming an emission height of 250 km. (d) Temporal evolution of the tips and valleys of the fingers during a ~7 min interval from 2030 to 2037 UT.

sources of ionospheric scintillation at high latitudes [*Moen et al.*, 2013, and references therein]. Here we briefly discuss the appearance of fingerlike structure in the trailing edge in connection with the generation of plasma irregularities within patches. In recent years, generation of patch-associated irregularities has been extensively studied by using in situ electron density measurements by rockets and low-altitude satellites. *Moen et al.* [2012] and *Oksavik et al.* [2012] employed in situ electron density measurements by the ICI-2 sounding rocket launched in the cusp and calculated the linear growth rate of GDI. They implied that structured soft particle precipitation in the cusp first creates kilometer-scale density perturbations and such relatively large-scale structures are subsequently broken down to meter-scale irregularities through the GDI process. More recent paper by *Goodwin et al.* [2015] questioned the generation of irregularities through GDI by using

in situ electron density measurements by the Swarm satellite. They showed that the amplitude of the density perturbation is larger near the cusp, probably due to the low-energy electron precipitation, and the fluctuations are much weaker on the nightside away from the cusp region. From this observation, they concluded, the patch-associated irregularities are directly produced by the cusp precipitation and GDI is not the primary production mechanism of patch-associated irregularities.

In contrast to the results of the above mentioned papers, *Hosokawa et al.* [2009] demonstrated that decameter-scale irregularities are distributed in the entire part of patches in the central polar cap region by using simultaneous measurements of 630.0 nm airglow patches and backscatter echoes of SuperDARN. This means that we need to explain why production of irregularities (i.e., plasma structuring process) is still active in the region away from the cusp (i.e., without soft particle precipitation). We suppose that the fingerlike structure identified during the current interval could be a key to answer this question. We claim that the fingerlike feature is a manifestation of the GDI process creating a few tens of kilometer-scale density structure. Such a few tens of kilometer-scale structures could be seed irregularities for producing further smaller irregularities through additional occurrence of GDI (i.e., cascading down to kilometer-scale or meter-scale irregularities). Although we are not able to image such smaller-scale structures by the ASI due to insufficient spatial and temporal resolutions, we suspect that a few tens of kilometer-scale irregularities can be further broken into smaller-scale irregularities through the GDI process. In order to confirm such a scenario, now we conduct numerical simulations of plasma structuring in the vicinity of patches and directly compare the simulation results with the optical observations. We also plan to investigate simultaneous observations of optical patches and patch-associated density irregularities by ground-based ASIs and in situ satellite measurement of the electron density for revealing the possible association between the fingerlike structure with small-scale density irregularities within patches.

Finally, the scale size of the fingers and flow distribution in their vicinity are estimated by tracking the tops and bottoms of the fingers for one of the patches (Patch D). The results are summarized in Figure 6. Figure 6a shows the all-sky image of Patch D at 2034 55s UT, and Figure 6b is a zoom in of Figure 6a where the outline of the trailing edge, the tips of the five fingers (T1 to T5), and the center of valleys between them (V1 to V4) are shown. The fingers appeared at around 2030 UT, and the patch disappeared from the FOV at around 2037 UT. Then, we are able to track the motion of the patch (i.e., divergence/convergence or rotation) for ~7 min by using the tips and valleys of the fingers as markers. The sampling of the tips and valleys has been done every 30 s. In the following, we discuss (1) horizontal scale size of the fingers, (2) motion of the fingers, and (3) evolution of the fingers, by using the traced position of the fingers. To derive the horizontal scale size of the fingers, first we map the traced outline of the trailing edge onto the horizontal plane assuming an emission height of 250 km (Figure 6c), and then we estimate the width of the five fingers. As indicated in Figure 6c, the width of the fingers ranges from 55 to 210 km. In addition, it is found that the length (scale size in the direction of extension) of the fingers is as large as 200 km (easternmost finger T1). These scale sizes would be fundamental parameters for evaluating the generation of fingers by reproducing the GDI structuring process using numerical simulation in the future.

Figure 6d shows how the tips and valleys of the fingers moved during the passage of Patch D across the FOV of the ASI. In general, the motions of the tips and valleys are very similar to each other, which means that the plasma convection behind the patch was rather uniform (i.e., no significant divergence/convergence). This result is not consistent with the work of *Nishimura et al.* [2013] who claimed an existence of high-speed localized flow channel within or in the vicinity of patches on the nightside. Regarding the rotation of the fingers, the traces of T4 and V3, and those of T5 and V4, respectively, show an overlap. This means that the fingers T4 and T5 experienced some rotation during their passage across the FOV. *Dahlgren et al.* [2012] indicated, by using data from the Resolute Bay incoherent scatter radar, rotational deformation of a patch on the dayside. Such rotational deformation of patches was first reported by *Oksavik et al.* [2010]. The current observation confirms that the rotational deformation of patches actually takes place in the central polar cap by tracking the shape of patches using the fingerlike structures as markers. In addition, it is possible to estimate the evolution of the fingerlike structures by tracking the motion of their tips and valleys. In Figure 6d, the profiles of the trailing edge are shown by the thick grey lines, respectively, for 2030 UT and 2037 UT. The separations between the tips and valleys are slightly larger at 2037 UT than those at 2030 UT. That is, the distance between the tips and valleys became slightly larger during the passage. This suggests that the fingers were still growing during the passage of Patch D across the FOV. At the moment, it is difficult to evaluate the time constant

of the evolution of fingers, but it would be possible to discuss the process in the future by comparing the numerical simulation of the GDI mechanism with the current observation.

In this paper, we only showed optical data during nighttime. However, optical observations are possible in Svalbard even on the dayside during midwinter period; thus, it is expected to detect similar structuring process on the dayside, especially near the cusp region. In the vicinity of the cusp, plasma flows are much more transient and contain lots of spatial structures (i.e., shears). In such a situation, the structuring process of patches may be different. *Carlson et al.* [2007] proposed a generation mechanism of patch-associated irregularities in which strong flow shears initially produce sheer driven instabilities near initial patch production, and subsequently the patch velocity slows and the GDI dominates. In the future, we plan to observe such a two-step structuring process of patches on the dayside by combining the high-time resolution optical data together with concurrent EISCAT and SuperDARN measurements.

5. Conclusion

We demonstrated, by using 2-D high-time resolution airglow measurements, that the gradient in the leading edge of patches is 2–3 times steeper than that in the trailing edge, which is consistent with the past satellite observations [*Coley and Heelis*, 1998] and simulations [e.g., *Gondarenko et al.*, 2003]. We also identified characteristic fingerlike structures in the trailing edge of the patches, which are probably created through GDI. From these observations, we suggest that the plasma structuring through GDI in the trailing edge stirs plasma across the boundary so that the gradient-scale length in the trailing edge becomes longer. Hence, the structuring through GDI can significantly affect the large-scale shape of patches. Although the observed asymmetry in the gradient can be qualitatively explained by the transport or mixing of plasma through GDI, we have not yet answered why the ratio of the gradient in the two edges is 2–3 during the current interval. This ratio may change as patches are advected deep into the dark hemisphere across the central polar cap. Namely, it is reasonable to expect that the ratio is close to 1 soon after their birth on the dayside and gradually increases during their travel across the polar cap region. In order to evaluate this prediction, we plan to conduct a statistical analysis of the gradients in the edges of patches observed by ASIs in the polar cap. Such a study of the patch edges contributes to the detailed understanding of the plasma structuring/irregularity generation within patches, which is very important in better predicting the space weather impacts of patches on the transionospheric communication links currently operative in the polar cap region. In addition, it was demonstrated that the fingerlike structures can be used as markers to estimate the fine-scale plasma flow within or in the vicinity of patches, which may enable us to understand the connection between the ionospheric convection in the polar cap and the substorm triggering mechanisms.

Acknowledgments

The authors would like to thank Fred Sigernes for his help at UNIS, Longyearbyen. We also thank Takeshi Aoki, a staff of Manufacturing Design Center for facilitating our work in the University of Electro-Communications. The ground optical data used in this paper can be provided on request to Satoshi Taguchi at Kyoto University. The authors wish to thank N. Ness at the Bartol Research Institute for access to data from MFI and SWE instruments on board the ACE spacecraft. The solar wind data from the ACE spacecraft can be accessed through the ACE science center at http://www.srl.caltech.edu/ACE/ASC/. This work was supported by Grants-in-Aid for Scientific Research (22340143 and 26302006) from the Japan Society for the Promotion of Science (JSPS).

References

Carlson, H. C. (2012), Sharpening our thinking about polar cap ionospheric patch morphology, research, and mitigation techniques, *Radio Sci.*, *47*, RS0L21, doi:10.1029/2011RS004946.

Carlson, H. C., T. Pedersen, S. Basu, M. Keskinen, and J. Moen (2007), Case for a new process, not mechanism, for cusp irregularity production, *J. Geophys. Res.*, *112*, A11304, doi:10.1029/2007JA012384.

Coley, W. R., and R. A. Heelis (1998), Structure and occurrence of polar ionization patches, *J. Geophys. Res.*, *103*, 2201–2208, doi:10.1029/97JA03345.

Crowley, G. (1996), Critical review of ionospheric patches and blobs, in *Review of Radio Science 1993–1996*, edited by W. R. Stone, pp. 619–648, Oxford Univ. Press, New York.

Dahlgren, H., G. W. Perry, J. L. Semeter, J.-P. St.-Maurice, K. Hosokawa, M. J. Nicolls, M. Greffen, K. Shiokawa, and C. Heinselman (2012), Space-time variability of polar cap patches: Direct evidence for internal plasma structuring, *J. Geophys. Res.*, *117*, A09312, doi:10.1029/2012JA017961.

Gondarenko, N. A., P. N. Guzdar, J. J. Sojka, and M. David (2003), Structuring of high latitude plasma patches with variable drive, *Geophys. Res. Lett.*, *30*(4), 1165, doi:10.1029/2002GL016437.

Goodwin, L. V., et al. (2015), Swarm in situ observations of F region polar cap patches created by cusp precipitation, *Geophys. Res. Lett.*, *42*, 996–1003, doi:10.1002/2014GL062610.

Hosokawa, K., K. Shiokawa, Y. Otsuka, A. Nakajima, T. Ogawa, and J. D. Kelly (2006), Estimating drift velocity of polar cap patches with all-sky airglow imager at Resolute Bay, Canada, *Geophys. Res. Lett.*, *33*, L15111, doi:10.1029/2006GL026916.

Hosokawa, K., K. Shiokawa, Y. Otsuka, T. Ogawa, J.-P. St-Maurice, G. J. Sofko, and D. A. Andre (2009), The relationship between polar cap patches and field-aligned irregularities as observed with an all-sky airglow imager at Resolute Bay and the PolarDARN radar at Rankin Inlet, *J. Geophys. Res.*, *114*, A03306, doi:10.1029/2008JA013707.

Hosokawa, K., J. I. Moen, K. Shiokawa, and Y. Otsuka (2011), Decay of polar cap patch, *J. Geophys. Res.*, *116*, A05306, doi:10.1029/2010JA016297.

Hosokawa, K., S. Taguchi, Y. Ogawa, and J. Sakai (2013), Two-dimensional direct imaging of structuring of polar cap patches, *J. Geophys. Res. Space Physics*, *118*, 6536–6543, doi:10.1002/jgra.50577.

Hosokawa, K., S. Taguchi, K. Shiokawa, Y. Otsuka, Y. Ogawa, and M. Nicolls (2014), Global imaging of polar cap patches with dual airglow imagers, *Geophys. Res. Lett.*, *41*, 1–6, doi:10.1002/2013GL058748.

Keskinen, M. J., and S. L. Ossakow (1983), Theories of high-latitude ionospheric irregularities: A review, *Radio Sci.*, *18*, 1077–1091, doi:10.1029/RS018i006p01077.

Khan, H., and S. W. H. Cowley (1999), Observations of the response time of high-latitude ionospheric convection to variations in the interplanetary magnetic field using EISCAT and IMP-8 data, *Ann. Geophys.*, *17*, 1306–1335.

Kivanc, O., and R. A. Heelis (1997), Structures in ionospheric number density and velocity associated with polar cap ionization patches, *J. Geophys. Res.*, *102*, 307–318, doi:10.1029/96JA03141.

Milan, S. E., M. Lester, and T. K. Yeoman (2002), HF radar polar patch formation revisited: Summer and winter variations in dayside plasma structuring, *Ann. Geophys.*, *20*, 487–499.

Moen, J., K. Oksavik, T. Abe, M. Lester, Y. Saito, T. A. Bekkeng, and K. S. Jacobsen (2012), First in-situ measurements of HF radar echoing targets, *Geophys. Res. Lett.*, *39*, L07104, doi:10.1029/2012GL051407.

Moen, J., K. Oksavik, L. Alfonsi, Y. Daabakk, V. Romano, and L. Spogli (2013), Space weather challenges of the polar cap ionosphere, *J. Space Weather Space Clim.*, *3*, A02, doi:10.1051/swsc/2013025.

Nishimura, Y., L. R. Lyons, K. Shiokawa, V. Angelopoulos, E. F. Donovan, and S. B. Mende (2013), Substorm onset and expansion phase intensification precursors seen in polar cap patches and arcs, *J. Geophys. Res. Space Physics*, *118*, 2034–2042, doi:10.1002/jgra.50279.

Oksavik, K., V. L. Barth, J. Moen, and M. Lester (2010), On the entry and transit of high-density plasma across the polar cap, *J. Geophys. Res.*, *115*, A12308, doi:10.1029/2010JA015817.

Oksavik, K., J. Moen, M. Lester, T. A. Bekkeng, and J. K. Bekkeng (2012), In situ measurements of plasma irregularity growth in the cusp ionosphere, *J. Geophys. Res.*, *117*, A11301, doi:10.1029/2012JA017835.

Prikryl, P., R. Ghoddousi-Fard, B. S. R. Kunduri, E. G. Thomas, A. J. Coster, P. T. Jayachandran, E. Spanswick, and D. W. Danskin (2013), GPS phase scintillation and proxy indices observed at high latitudes during a moderate geomagnetic storm, *Ann. Geophys.*, *31*, 805–816, doi:10.5194/angeo-31-805-2013.

Shiokawa, K., Y. Otsuka, and T. Ogawa (2009), Propagation characteristics of nighttime mesospheric and thermospheric waves observed by optical mesosphere thermosphere imagers at middle and low latitudes, *Earth Planets Space*, *61*, 479–491.

Taguchi, S., K. Hosokawa, Y. Ogawa, T. Aoki, and M. Taguchi (2012), Double bursts inside a poleward-moving auroral form in the cusp, *J. Geophys. Res.*, *117*, A12301, doi:10.1029/2012JA018150.

Weber, E. J., J. Buchau, J. G. Moore, J. R. Sharber, R. C. Livingston, J. D. Winningham, and B. W. Reinisch (1984), *F* layer ionization patches in the polar cap, *J. Geophys. Res.*, *89*, 1683–1694.